Phase equilibria of an Al$_{0.5}$CrFeCoNiCu High Entropy Alloy

N.G. Jones *, A. Frezza, H.J. Stone

Department of Materials Science and Metallurgy, University of Cambridge, 27 Charles Babbage Road, Cambridge CB3 0FS, UK

ABSTRACT

The phase equilibria of an Al$_{0.5}$CrFeCoNiCu High Entropy Alloy has been studied following 1000 h exposures at 700, 850 and 1000 °C. Above 1000 °C, the material comprised of two *fcc* solid solutions, one a multi-element phase and the other a Cu rich phase. Below 1000 °C, the *fcc* phases persisted, but were accompanied by the formation of two intermetallic compounds. In contrast to previous reports, the L1$_2$ phase was also found to precipitate through a solvus at ~850 °C. The results indicated that a solid state single phase field does not exist in this material at any temperature and all of the observed phases could be rationalised with reference to existing phase diagrams. This suggests that configurational entropy does not overcome the enthalpic contribution to the Gibbs energy, which governs phase equilibria of this alloy.

© 2014 The Authors. Published by Elsevier B.V. This is an open access article under the CC BY license (http://creativecommons.org/licenses/by/3.0/).

1. Introduction

High Entropy Alloys (HEAs) are an intriguing new class of metallic materials, based on a novel approach to materials design. Contrary to conventional alloying, these materials do not have a principle component, but are instead based on near equiatomic mixtures of five or more elements [1,2]. Traditional metallurgical wisdom would expect the microstructure of these materials to contain a number of intermetallic phases, yet surprisingly, this has not been the case. Experimental studies have reported single or dual phase as-cast microstructures [2–5], and corresponding diffraction data have indicated that these phases have simple crystal structures, such as *fcc* or *bcc*.

To rationalise these observations, it has been postulated that the entropy of mixing in these multi-component systems must be very high, resulting in entropically stabilised solid solution phases [1,2]. The basis for this hypothesis lies in classical thermodynamics, where the entropy of mixing between two soluble components is at its maximum when the constituent elements are in equiatomic concentrations. If this idea is extended and perfect mixing is assumed, then the statistical entropy of a material can be expressed as $R \ln n$, where R is the gas constant and n is the number of elemental components within the system [1,2]. Using this relationship, it can be seen that the entropy of an equiatomic multi-component system would be expected to increase with the number of constituent elements.

Over the last decade, HEAs have received a significant level of attention and a considerable number of manuscripts now exist reporting on a vast range of elemental combinations. However, despite this extensive body of research, it remains unclear as to whether these multi-component solid solutions are actually thermodynamically stable.

Many studies report that relatively short thermal exposures do not affect the microstructures of these alloys, or that solidification induced microsegregation leads to the formation of additional stabilised phases [6–9]. However, a growing number of manuscripts are reporting evidence of phase evolution/decomposition. Specifically, precipitation has been observed in some alloys following exposure at elevated temperatures [10–15] and age hardening, which is indicative of microstructural evolution, has also been reported [10,16,17].

One of the difficulties in assessing thermodynamic stability from the existing literature is the wide range of compositions reported and the variation in thermal treatments. The diffusion kinetics of HEAs are not well established, but are thought to be slow [15,18,19], and therefore significant exposure times would be required to reach equilibrium. In addition, hot and cold working operations are often employed, making it difficult to separate thermodynamic processes from thermomechanically assisted effects. For instance, the phase evolution of Al$_{0.5}$CrFeCoNiCu during heat treatment at 700, 900 and 1100 °C has previously been reported [15]. However, this material was cold rolled and annealed prior to thermal exposure. Despite the first interpass heat treatment being only 1 h at 900 °C, a new phase formed in the material, which not only makes the interpretation of subsequent thermal exposures difficult, but also suggests that the diffusional kinetics may not be as sluggish as widely thought.

* Corresponding author. Tel.: +44 1223 334367.
E-mail address: ngj22@cam.ac.uk (N.G. Jones).

To date, the most comprehensive investigation of phase stabilisation by configurational entropy involved the systematic substitution of elements in the single phase CoCrFeMnNi alloy [20]. Each variation replaced one of the constituent elements with a nominally equivalent species, based on the Hume-Rothery rules, such that the entropy of mixing remained constant. In contrast to the base alloy, all of the variant alloys contained multiple phases, leading the authors to conclude that compositional complexity is not the dominating factor in determining the stability of these materials.

Recently, we demonstrated that the free energy curve of $Al_{0.5}CrFeCoNiCu$ contains a miscibility gap with two local minima, rather that the single minima of a solid solution [21]. As such, the configurational entropy of this material is insufficient to fully stabilise a single solid solution phase, making the material susceptible to phase decomposition during heat treatment. The formation of intermetallic phases at intermediate temperatures has previously been reported in this alloy [15]. However, these findings disagreed with the phase diagram proposed in Fig. 10 of Ref. [3]. Critically, it was suggested that the alloy solidified as three phases, two *fcc* phases and an $L1_2$ phase in Ref. [15], whilst Refs. [21,3] both report only two *fcc* phases.

In order to resolve these inconsistencies, we report on the elemental partitioning and phase equilibria of $Al_{0.5}CrFeCoNiCu$ following 1000 h exposures at 700, 850 and 1000 °C from the as-cast state. Careful microstructural characterisation, using a number of techniques, has been used to identify the constituent phases formed at each temperature. Whilst the phases observed are broadly consistent with previous reports [15], our interpretation of the phase boundaries is significantly different, particularly with respect to the formation of the $L1_2$ phase, which we show forms via a solid state precipitation process below ~850 °C.

2. Experimental methods

A 40 g ingot of $Al_{0.5}CrFeCoNiCu$ was created from pure elemental metals ($\geq$ 99.95%) via arc melting in an inert atmosphere. To increase ingot homogeneity, the alloy was inverted and remelted a total of five times. Three, 10 mm lengths were cut from the as-cast ingot, encapsulated in an inert atmosphere and heat treated for 1000 h at 700, 850 and 1000 °C respectively. All samples were water quenched following the thermal exposure.

Microstructural characterisation was conducted using back-scattered electron imaging (BSEI) in a JEOL 5800 Scanning Electron Microscope. Qualitative compositional mapping and quantitative point analyses were performed in the same instrument using an Oxford Instruments energy dispersive X-ray (EDX) spectroscopy system. Bulk compositions were determined by averaging data from five large area ($\sim 500 \times 500$ μm) scans, whilst individual phase compositions were determined from the average of five point analyses.

Macroscopic crystallographic information was obtained via X-ray diffraction using a Philips PW1050 diffractometer in Bragg–Brentano geometry with CuKα radiation. Data was collected between 20° and 120° 2θ in 0.04° steps with a 20 s counting period. Differential Scanning Calorimetry (DSC) was performed between room temperature and 1450 °C under flowing argon using a Netzsch 404 high temperature calorimeter at heating and cooling rates of 10 °C min^{-1}.

3. Results

The microstructure of the as-cast alloy is shown in Fig. 1 and is typical of a material that has undergone dendritic solidification.

The interdendritic material was rich in heavy elements and showed evidence of shrinkage porosity. Bulk compositional assessment showed that each of the constituent elements were within 1 at% of the nominal composition. The distribution of each element in the as-cast state is shown in Fig. 2. Cr, Fe and Co were observed to have partitioned to the dendrites, whilst the interdendritic material consisted predominately of Cu. Ni and Al were more evenly distributed between the two phases, although Ni concentrations were higher in the dendrites and Al levels were greater in the interdendritic material. Such observations are consistent with previous reports [3,21], and quantified compositions for the two phases are given in Table 1. In addition, the elemental distribution maps showed a compositional gradient in the dendrites, from core to edge, indicative of conventional solidification induced microsegregation.

X-ray diffraction data obtained from the as-cast structure is shown in Fig. 3a. All of the high intensity peaks could be assigned to an *fcc* structure, whilst the low intensity peaks could not be conclusively indexed. The corresponding microstructure, shown in Fig. 1, was dominated by the dendrites and thus it is reasonable to conclude that these must be giving rise to *fcc* reflections in the X-ray spectrum. Importantly, the area ratio of the low intensity peaks was inconsistent with the volume fraction of interdendritic material observed. Detailed examination of the *fcc* peak line profiles showed distinct broadening around the base of the peak and shouldering on the low two theta side. These features suggest that the *fcc* reflections originate from two phases with extremely similar lattice parameters.

To separate the two different contributions, each diffraction peak was fitted with two profile functions using a non-linear least squares algorithm in Wavemetrics Igor Pro. To account for diffraction from both CuKα$_1$ and CuKα$_2$ radiation, each profile function contained two Gaussian peaks, with the relative position, intensity and width of the CuKα$_1$ and CuKα$_2$ peaks constrained, such that each profile function had only three fitting variables. An example of a fitted peak and the contributing profile functions is shown in Fig. 3b and indicates the presence of two *fcc* structures in the material. The refined profile positions of every reflection for each phase were used to obtain their lattice parameters through a non-linear least squares minimisation, given in Table 2. Previous studies of this material using transmission electron microscopy have also shown the presence of $L1_2$ precipitates, which were thought to have formed within the dendrites upon cooling [3,21] and the structure of this phase was consistent with many of the low intensity reflections observed in the diffraction data.

Representative microstructures of $Al_{0.5}CrFeCoNiCu$ following 1000 h heat treatment at 700, 850 and 1000 °C are shown Fig. 4. Precipitates were observed in the 700 and 850 °C micrographs, clearly indicating that the alloy had undergone phase decomposition, whilst the microstructure of the sample exposed at 1000 °C bore a close resemblance to that of the as-cast material. To assist in identifying the phases present in the microstructures, elemental distribution maps for each of the heat treatment temperatures were obtained and are shown in Figs. 5–7. Corresponding quantitative compositional measurements of each phase are given in Table 1.

The elemental distribution map following exposure at 700 °C is shown in Fig. 5, from which four distinct microstructural constituents of different composition can be identified. The dendrites remained a multi-component phase dominated by Cr, Fe, Co and Ni. The composition of this phase was similar to that in the as-cast, although there was a greater concentration of Cu. In contrast, the composition of the interdendritic material had changed markedly when compared to the as-cast material. Following heat treatment the interdendritic material had become significantly enriched in Cu and exhibited limited solubility for all the other constituent
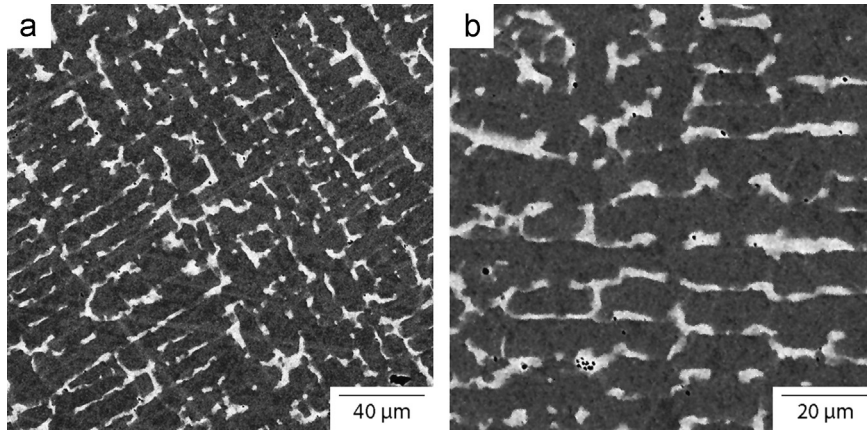
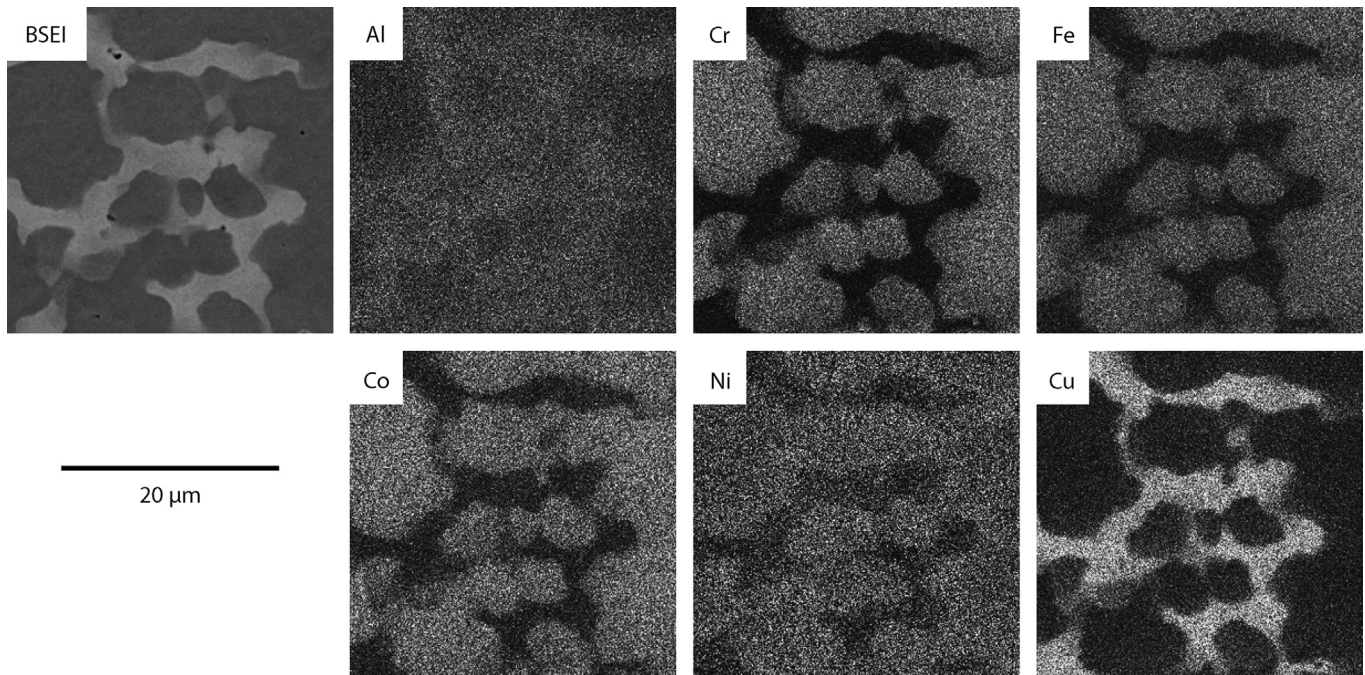**Fig. 1.** BSEI of $Al_{0.5}CrFeCoNiCu$ in the as-cast state showing a dendritic microstructure.

Fig. 2. EDX determined elemental distribution map of $Al_{0.5}CrFeCoNiCu$ in the as-cast state.

elements, particularly Cr, Fe and Co. Correspondingly, at the interfaces between the dendrites and the interdendritic material, two new phases had formed. The black precipitates seen in the BSEI image were a Ni and Al rich phase (identified as Precipitate 1 in Table 1), whilst regions of a Cr rich phase, which contained significant levels of Fe and Co, could also be observed (identified as Precipitate 2 in Table 1).

Following heat treatment at 850 °C the element partitioning, shown in Fig. 6, was found to be similar to that of the 700 °C treated sample. Again, the material appeared to consist of four phases; a multi-component dendrite, a Ni and Al rich precipitate, a Cr rich precipitate and a Cu rich interdendritic phase. However, heat treatment at the higher temperature had altered the extent of the element partitioning in some of the phases. After exposure at 850 °C the dendrites contained more Cr and less Cu and Al than observed at 700 °C, whilst the interdendritic material exhibited greater solubility for Al and Ni. In contrast, the compositions of the two precipitate phases were largely unaltered by the change in exposure temperature. Within the dendrites, Cu-rich, Al containing precipitates were also observed at 850 °C. The composition of these precipitates was similar to the interdendritic material, and

their formation away from the interface region is thought to be a result of the diffusional distance limits of participating atomic species within the dendrites.

As previously mentioned, the microstructure obtained following heat treatment at 1000 °C showed a close resemblance to that of the as-cast material. The elemental distribution maps shown in Fig. 7 indicated that there were two phases in the microstructure; Ni, Co, Fe, Cr rich dendrites and Cu rich interdendritic material, with similar volume fractions to the as-cast material. The phase boundaries in the 1000 °C microstructure were sharper than those in the as-cast material, Fig. 2, and the phase composition analysis revealed that further partitioning had occurred such that concentration of Co, Fe and Cr in the interdentritic material had reduced.

X-ray diffraction spectra from the heat treated samples are shown in Fig. 8. All the spectra contained the double *fcc* peaks corresponding to the dendritic and interdendritic phases seen in the as-cast material, Fig. 3. Following exposure at 1000 °C, the microscopy and element distribution maps suggested that the microstructure contained only two phases, whereas the X-ray spectrum contained additional peaks at low angles. These were again attributed to the presence of an $L1_2$ superlattice phase, formed on cooling from the

Table 1
Phase compositions in at% determined using EDX.

Phase	Al	Cr	Fe	Co	Ni	Cu
Dendrite						
As-cast	6.2	23.4	23.4	20.9	17.4	9.1
700 °C	6.6	20.4	21.9	19.8	18.5	12.8
850 °C	3.9	24.1	24.9	22.0	16.6	8.4
1000 °C	7.0	22.8	22.8	20.4	18.7	8.5
Interdendritic						
As-cast	12.1	7.0	7.2	6.9	15.8	51.0
700 °C	4.8	1.9	2.3	2.5	6.3	82.3
850 °C	9.9	1.9	2.6	2.7	11.0	71.8
1000 °C	11.4	3.5	5.2	5.0	15.7	59.5
Precipitate 1						
As-cast	–	–	–	–	–	–
700 °C	31.8	2.5	8.3	10.7	38.7	8.0
850 °C	31.1	3.7	7.8	10.0	35.5	11.9
1000 °C	–	–	–	–	–	–
Precipitate 2						
As-cast	–	–	–	–	–	–
700 °C	0.5	52.1	23.2	19.1	4.4	0.7
850 °C	0.8	53.0	21.5	18.6	5.5	0.6
1000 °C	–	–	–	–	–	–

Table 2
Least squares refined phase lattice parameters in Å (± 0.005 in all cases).

Phase	Structure	As-cast	700 °C	850 °C	1000 °C
Dendrite	fcc	3.595	3.587	3.591	3.594
Interdendritic	fcc	3.602	3.613	3.617	3.620
Precipitate 1	B2	–	2.882	2.884	–
Precipitate 2	D8$_b$	–	8.800	8.805	–
		–	4.562	4.557	–
Precipitate 3	L1$_2$	3.628	3.614	–	3.603

heat treatment temperature. The L1$_2$ reflections were also present in the 700 °C spectrum, but notably absent in the 850 °C pattern. The diffraction spectra from the 700 and 850 °C samples also contained extra peaks, related to the precipitates observed in Figs. 5 and 6. A set of reflections corresponding to a B2 structure were indexed in both samples, but the remaining unassigned peaks were insufficiently distinct to unambiguously determine the other crystal structure. The area of the B2 peaks was significantly greater than those of the unidentified precipitate, which suggested that there was a higher fraction of this phase in the microstructure. Figs. 4–6 show that the samples contained a significantly greater volume of the Ni and Al rich precipitates than the Cr rich precipitates. Given that the composition of these precipitates was close to that NiAl, which has a B2 crystal structure, it is reasonable to associate this phase with the B2 reflections. From the composition data in Table 1, the Cr rich precipitates were dominated by Cr, Fe and Co. When the measured composition was plotted on the relevant sections of the ternary phase diagrams at 700 °C and 850 °C [22], the precipitates lay within the σ phase field. The D8$_b$ structure of this phase could account for the remaining low intensity diffraction peaks.

The thermograms obtained using DSC for each sample are shown in Fig. 8. A large endothermic peak was observed in all cases at a temperature around 1350 °C, which corresponded to the melting of the dendrites. A second, smaller endothermic peak also occurred at around 1125 °C, associated with the incipient melting of the Cu rich interdendritic material. The thermograms from the 700 and 850 °C aged material show an additional, broad endothermic peak between 850 and 1100 °C. This was attributed to the dissolution of the B2 and σ phases, seen in the heat treated microstructures, Fig. 4. At temperatures around 850 °C, a sigmoidal deviation in heat flow occurred in the thermograms of the as-cast, 700 and 1000 °C heat treated samples. A similar feature is commonly observed in the thermograms of Ni-base superalloys and corresponds to the formation of the L1$_2$ γ′ phase from the *fcc* γ phase [23]. An L1$_2$ phase is known to form in this material when quenched from 1000 °C [15], and superlattice reflections were observed in the X-ray diffraction patterns of the as-cast, 700 and 1000 °C aged samples, Figs. 3 and 8. Therefore, this deviation was attributed to the dissolution of the L1$_2$ phase.

A summary of the experimentally determined phase equilibria of Al$_{0.5}$CrFeCoNiCu is provided in Table 3, and these results show some similarity to those of Ng et al. (see Fig. 8 in Ref. [15]). However, there are also some critical differences. In this study, no evidence of a *bcc* phase was found and it is likely that the *bcc* and *ordered bcc* phases reported in Ref. [15] are the B2 phase observed here. Ng et al. [15] also proposed that an *ordered fcc* phase was present at all temperatures below the solidification temperature. Whilst an L1$_2$ phase was observed in the as-cast, 700 and 1000 °C samples of the present study, the DSC thermograms shown in Fig. 9, indicated that the solvus temperature was ~850 °C. Therefore, the L1$_2$ phase can only be thermodynamically stable below this temperature and must have formed during cooling in the as-cast and 1000 °C aged samples. Again, this is consistent with conventional Ni-base superalloy metallurgy, where γ′ formation cannot be suppressed by quenching [24–27]. However, it should be
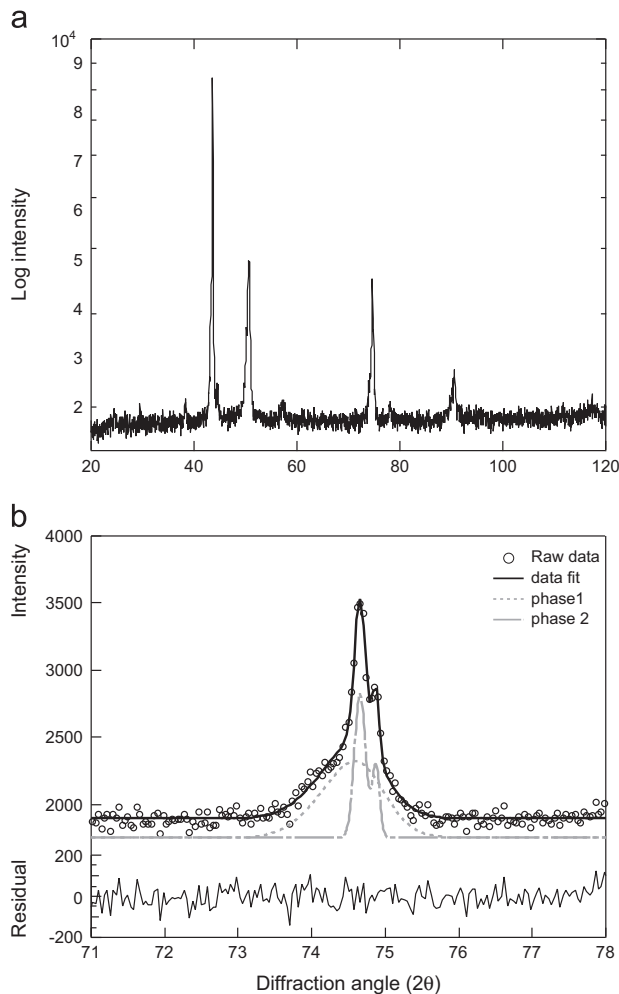

Fig. 3. (a) X-ray diffraction spectrum of Al$_{0.5}$CrFeCoNiCu in the as-cast state and, (b) the {220} reflection fitted with two peak profile functions, each accounting for Kα$_1$ and Kα$_2$ contributions.
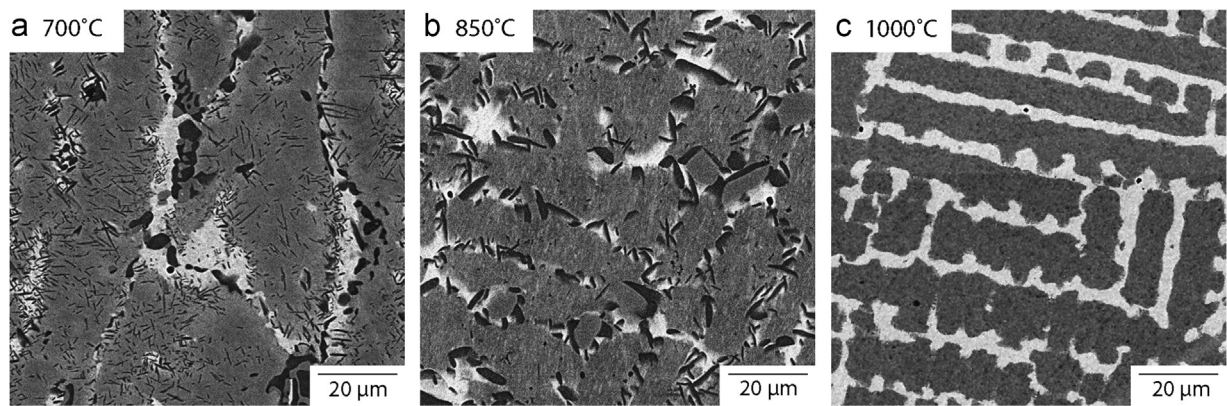
Fig. 4. BSEI micrographs of $Al_{0.5}CrFeCoNiCu$ following 1000 h heat treatment at (a) 700 °C, (b) 850 °C, and (c) 1000 °C.

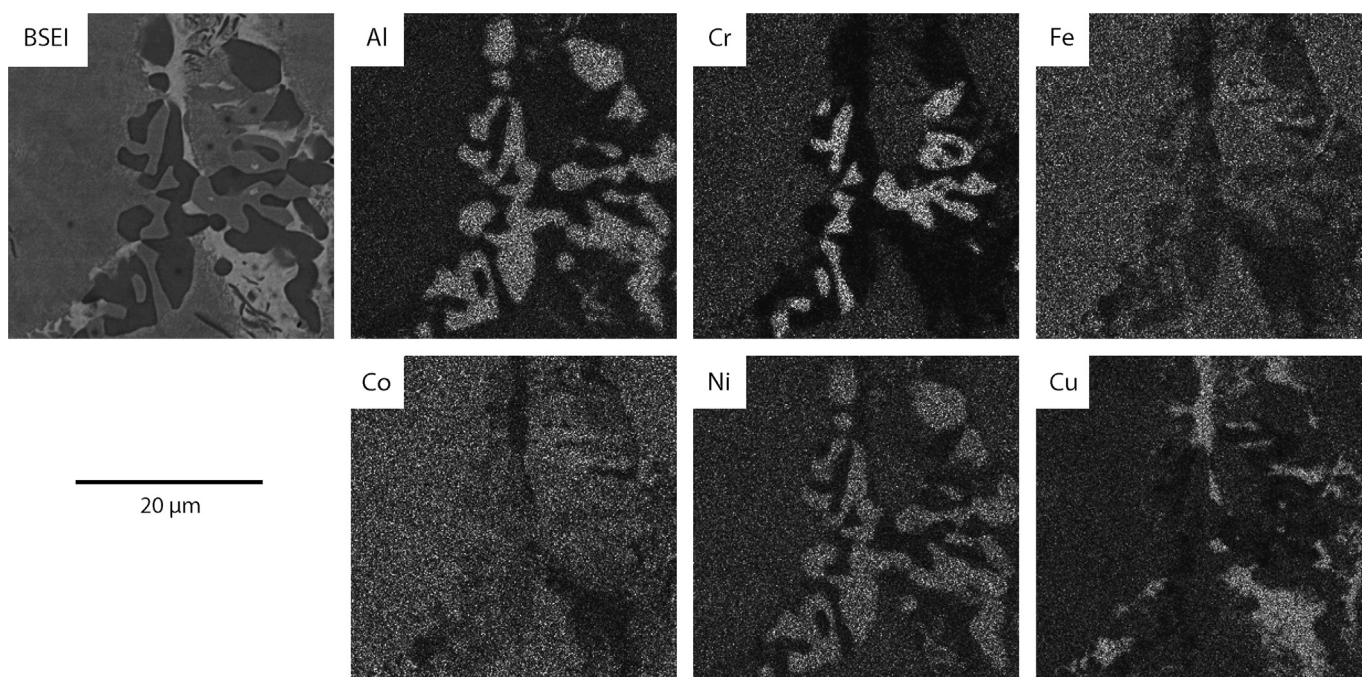**Fig. 5.** BSEI of $Al_{0.5}CrFeCoNiCu$ following 1000 h heat treatment at 700 °C and corresponding element distribution maps determined using EDX.

noted that the $L1_2$ phase did not persist following all heat treatments. The X-ray diffraction pattern of the 850 °C heat treated sample, Fig. 8, contained no $L1_2$ superlattice reflections, nor was there a sigmoidal feature in the corresponding DSC thermogram, Fig. 9. Since the $L1_2$ phase has been reported to form in the dendrites [3,21], it is important to consider how the phase chemistry varied with temperature. The EDX data in Table 1 showed a significant reduction in the Al content of the dendrites at 850 °C, when compared with those found at both 700 and 1000 °C. Therefore, it is proposed that the concentration of Al in the dendrites at 850 °C was below the critical level for an ordering induced phase formation, and hence why the $L1_2$ phase was not observed.

4. Discussion

To date, the majority of HEA studies have reported as-cast microstructures with two phases, both of which exhibit simple crystal structures. Many of these studies suggest that these phases are entropically stabilised solid solutions, although this would seem unlikely given the microstructural decomposition reported here. Furthermore, it has recently been demonstrated that a single solid state phase field does not exist in this alloy and that enthalpy dominates the associated thermodynamics [21]. Therefore, it should be possible to rationalise the observed phase equilibria by reference to established phase diagrams.

The elemental partitioning and phase assembly observed in the as-cast and 1000 °C samples were extremely similar, which suggested that the solidification phases are the thermodynamically stable high temperature phases and not simply a product of solidification induced microsegregation. Therefore, the phase evolution of both material conditions can be considered together. In the solid state, there is little to no solubility for Cu in Cu–Cr, Cu–Fe, or Cu–Co alloys [28–30], and therefore its demixing to form an additional phase is not surprising. However, Cu solid solutions may contain up to $\sim$20 at% Al [31], and complete solubility is observed between Ni and Cu [32]. Similarly, Ni–Co–Fe shows almost complete solubility above 800 °C [33], and whilst the ternary diagrams of Ni/Co/Fe with Cr exhibit multiphase regions, the solubility of Cr in each Ni/Co/Fe binary solid solutions at elevated temperatures is always significant [22,34–36]. The
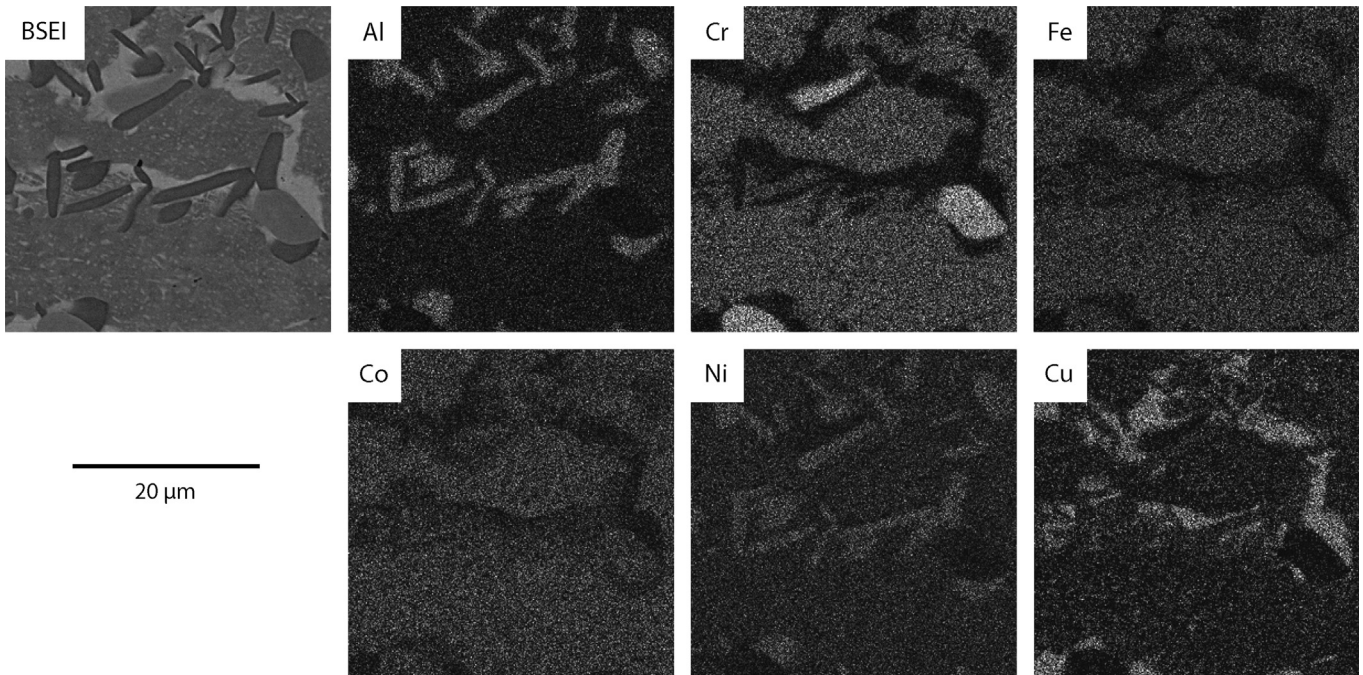
Fig. 6. BSEI of $Al_{0.5}CrFeCoNiCu$ following 1000 h heat treatment at 850 °C and corresponding element distribution maps determined using EDX.
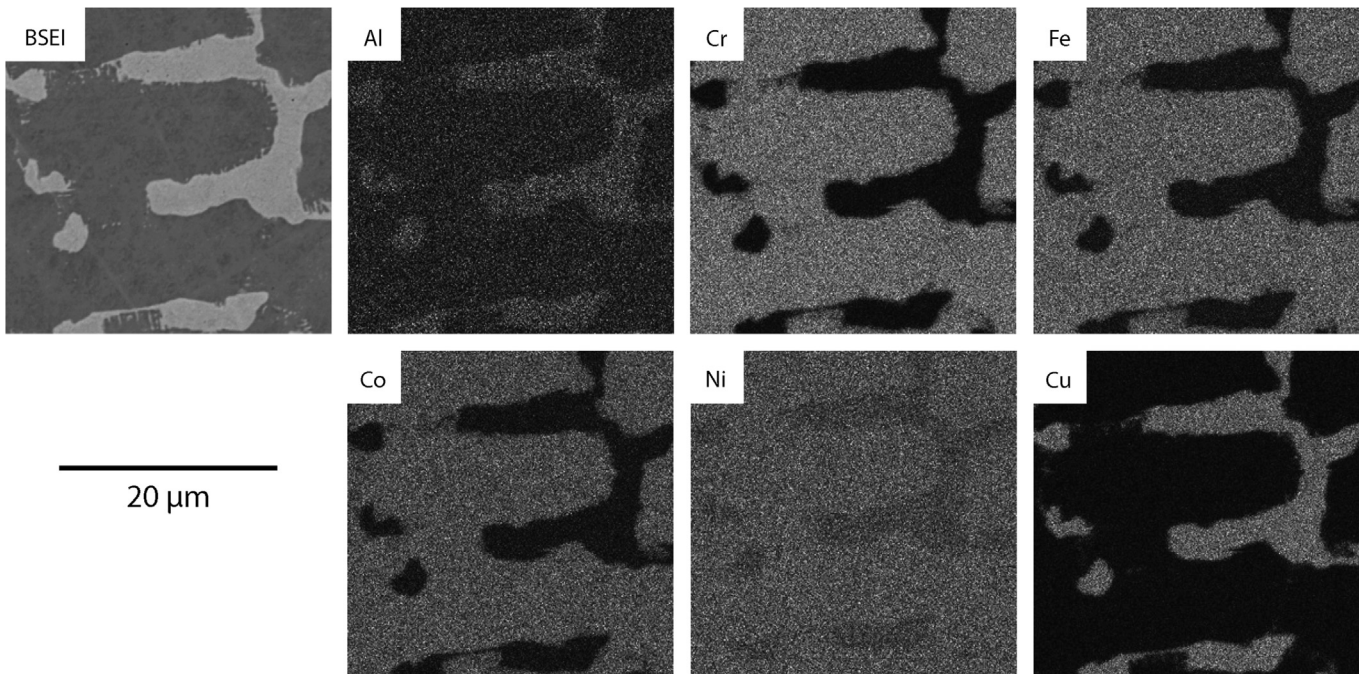

Fig. 7. BSEI of $Al_{0.5}CrFeCoNiCu$ following 1000 h heat treatment at 1000 °C and corresponding element distribution maps determined using EDX.

solubility of Al in binary mixtures of Ni/Co/Fe/Cr is more restricted, but is typically ≥ 10 at% at temperatures above 1000 °C [37–42]. Thus, the elemental partitioning observed in the as-cast and 1000 °C samples, Figs. 2 and 7, is entirely consistent with existing phase diagrams.

Given that $Al_{0.5}CrFeCoNiCu$ consists of two phases at high temperature, where the entropic term should dominate the Gibbs energy, the precipitation of additional intermetallic phases at lower temperatures, where the enthalpy would become increasingly significant, seems entirely logical. The composition of the dendritic material, given in Table 1, was similar at all temperatures, suggesting that this phase field extended from initial

solidification to room temperature. In contrast, the interdendritic material rejected all other constituent elements, and became increasingly Cu rich at lower temperatures. Therefore, when heat treated at 700 and 850 °C, an increased concentration of Cr, Fe, Co, Ni and Al would have been produced at the interface between the dendrite and interdendritic phases. NiAl is well known to have a large enthalpy of formation and, as a betholide, can accommodate significant levels of substitutions on its two sub-lattices. In particular, the B2 phase fields in the Ni–Al–Fe and the Ni–Al–Co systems are broad and span across the respective ternary phase diagrams [37,40,41,43]. However, the solubility for Cr within the NiAl phase is very low and, thus, the formation of the B2
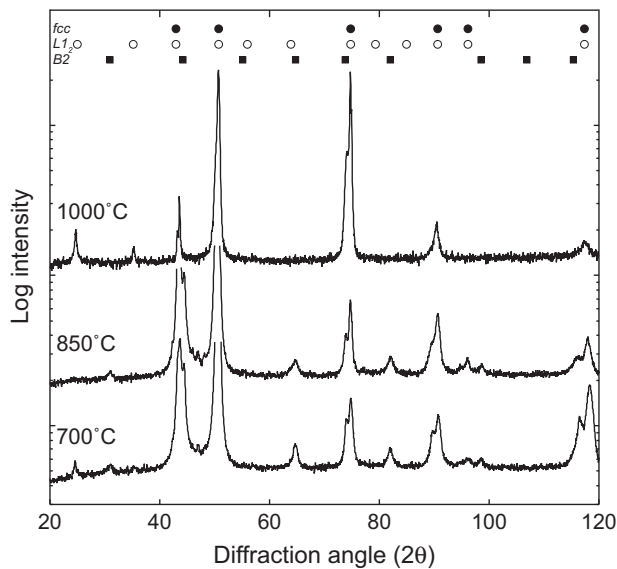
Fig. 8. X-ray diffraction spectra of Al$_{0.5}$CrFeCoNiCu following 1000 h heat treatment at 700, 850 and 1000 °C. Reflection markers; *fcc* – filled circles, L1$_2$ – open circles and B2 – filled squares.

Table 3
Summary of equilibrium phases observed at the investigated temperatures.

Phase	700 °C	850 °C	1000 °C
fcc$_1$	✓	✓	✓
fcc$_2$	✓	✓	✓
B2	✓	✓	✗
σ	✓	✓	✗
L1$_2$	✓	✗	✗

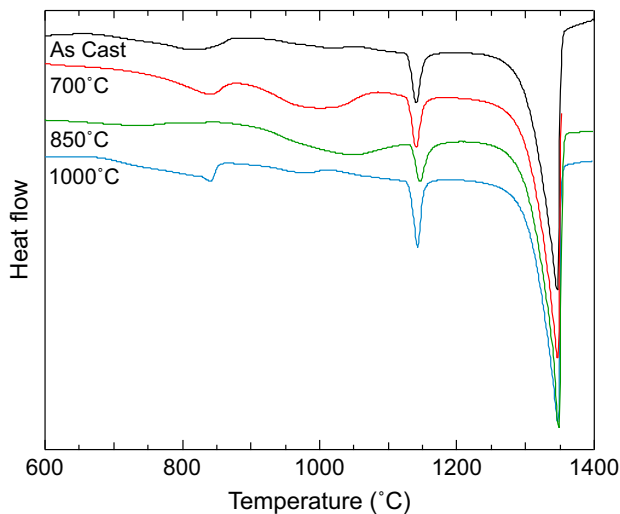**Fig. 9.** DSC thermograms for Al$_{0.5}$CrFeCoNiCu in the as-cast condition and following 1000 h heat treatment at 700 °C, 850 °C and 1000 °C.

intermetallic would be expected to cause the surrounding material to become further enriched in Cr [44].

Within the 700–1000 °C temperature range considered in this study, the binary solubility of Co and Fe in Cr varies from ~5 to 15 and 30 to 80 at% respectively. However, ternary combinations do not produce a large solid solution phase field. Instead, higher concentrations of Co and Fe form the σ phase. Therefore, its precipitation at the interface between the interdendritic material

and the B2 phase, where the local concentrations of Cr, Co and Fe were elevated, is also consistent with known phase equilibria.

Given that, the dendrite composition remained reasonably constant across the entire range of temperatures studied, whilst the interdendritic phase showed significant variation, particularly in the concentration of Ni and Al, it seems likely that the formation of intermetallic phases in this alloy is principally driven by the solubility limits of the constituent elements in Cu at any given temperature.

5. Conclusions

The phase equilibria of an Al$_{0.5}$CrFeCoNiCu High Entropy Alloy has been established following 1000 h heat treatments at 700, 850 and 1000 °C. At temperatures above 1000 °C the material consists of two phases, one a multiple element solid solution and the other a Cu rich solid solution. Both phases have an *fcc* crystal structure, with very similar lattice parameters. These phases are stable up to their melting temperatures, which are ~1150 °C for the Cu based solid solution and ~1350 °C for the multi-component phase. At temperatures below 1000 °C the reduced solubility of the constituent elements in the Cu rich solid solution causes the precipitation of two intermetallic phases, a NiAl based B2 compound and the D8$_b$, σ phase. In addition, and in contrast to previous studies of this alloy, the L1$_2$ phase was shown to form when cooled through a solvus at ~850 °C. Whilst evidence of this phase also existed in the as-cast and 1000 °C samples, it was believed to have formed during cooling, as with γ′ in Ni-base superalloys.

The precipitation of intermetallic phases during thermal exposure indicates that enthalpic terms dominate the behaviour of this material, in agreement with the conclusions of Ref. [21]. In addition, all of the observed phases could be rationalised by simply considering existing binary and ternary phase diagrams. This suggests that configurational entropy does not overcome the enthalpic contribution to the Gibbs energy, which governs phase equilibria of this alloy.

References

[1] J. Yeh, High-Entropy Multielement Alloys, US Patent App. 10/133,495, 2002.
[2] J. Yeh, S. Chen, S. Lin, J. Gan, T. Chin, T. Shun, C. Tsau, S. Chang, Adv. Eng. Mater. 6 (2004) 299–303.
[3] C. Tong, Y. Chen, S. Chen, J. Yeh, T. Shun, C. Tsau, S. Lin, S. Chang, Metall. Mater. Trans. A-Phys. Metall. Mater. Sci. 36A (2005) 881–893.
[4] B. Cantor, I.T.H. Chang, P. Knight, A.J.B. Vincent, Mater. Sci. Eng.: A 375–377 (2004) 213–218.
[5] C.-C. Tung, J.-W. Yeh, T.-T. Shun, S.-K. Chen, Y.-S. Huang, H.-C. Chen, Mater. Lett. 61 (2007) 1–5.
[6] O.N. Senkov, G.B. Wilks, D.B. Miracle, C.P. Chuang, P.K. Liaw, Intermetallics 18 (2010) 1758–1765.
[7] C.-M. Lin, H.-L. Tsai, H.-Y. Bor, Intermetallics 18 (2010) 1244–1250.
[8] L.H. Wen, H.C. Kou, J.S. Li, H. Chang, X.Y. Xue, L. Zhou, Intermetallics 17 (2009) 266–269.
[9] C.-M. Lin, H.-L. Tsai, Mater. Chem. Phys. 128 (2011) 50–56.
[10] S.-T. Chen, W.-Y. Tang, Y.-F. Kuo, S.-Y. Chen, C.-H. Tsau, T.-T. Shun, J.-W. Yeh, Mater. Sci. Eng. A 527 (2010) 5818–5825.
[11] C.-M. Lin, H.-L. Tsai, Intermetallics 19 (2011) 288–294.
[12] T.-T. Shun, Y.-C. Du, J. Alloys Compd. 479 (2009) 157–160.
[13] C.-W. Tsai, M.-H. Tsai, J.-W. Yeh, C.C. Yang, J. Alloys Compd. 490 (2010) 160–165.
[14] C.-M. Lin, H.-L. Tsai, J. Alloys Compd. 489 (2010) 30–35.
[15] C. Ng, S. Guo, J. Luan, S. Shi, C.T. Liu, Intermetallics 31 (2012) 165–172.

[16] T.-T. Shun, Y.-C. Du, J. Alloys Compd. 478 (2009) 269–272.
[17] T.-T. Shun, C.-H. Hung, C.-F. Lee, J. Alloys Compd. 495 (2010) 55–58.
[18] J.-W. Yeh, Ann. Chim. – Sci. Mater. 31 (2006) 633–648.
[19] K.Y. Tsai, M.H. Tsai, J.W. Yeh, Acta Mater. 61 (2013) 4887–4897.
[20] F. Otto, Y. Yang, H. Bei, E.P. George, Acta Mater. 61 (2013) 2628–2638.
[21] N.G. Jones, J.W. Aveson, A. Bhowmik, B.D. Conduit, H.J. Stone, Intermetallics 54 (2014) 148–153.
[22] G. Raynor, V. Rivlin, Phase Equilibria in Iron Ternary Alloys, 1988, pp. 213–230.
[23] D.L. Sponseller, Superalloys 1996 (1996) 259–270.
[24] D.U. Furrer, H.-J. Fecht, Scr. Mater. 40 (1999) 1215–1220.
[25] S.S. Babu, M.K. Miller, J.M. Vitek, S.A. David, Acta Mater. 49 (2001) 4149–4160.
[26] R.D. Kissinger, Superalloys 1996 (1996) 687–695.
[27] E.H. Van Der Molen, J.M. Oblak, O.H. Kriege, Metall. Trans. A 2 (1971) 1627–1633.
[28] M. Leonov, N. Bochvar, V. Ivanchenko, Dokl. Akad. Nauk SSSR 290 (1986) 888–890.
[29] S.-E. Amara, A. Belhadj, R. Kesri, S. Hamar-Thibault, Z. Metallkunde 90 (1999) 116–123.
[30] T. Nishizawa, K. Ishida, J. Phase Equilibria 5 (1984) 161–165.
[31] X. Liu, I. Ohnuma, R. Kainuma, K. Ishida, J. Alloys Compd. 264 (1998) 201–208.
[32] L. Palatnik, N. Gladkikh, Dokl. Akad. Nauk SSSR 140 (1961) 1297.
[33] G. Raynor, V. Rivlin Equilibria in Iron Ternary Alloys, 1988, pp. 247–255.
[34] T. Chart, A. Dinsdale, F. Putland, The NPL ALLOYDATA Bank: Its Use in the Calculation of Phase Diagrams for Super-Alloy Development, in: Special Publication-Chemical Society, 1980, pp. 235–245.
[35] K. Gupta, S. Rajendraprasad, A. Jena, R. Sharma, Trans. Indian Inst. Met. 37 (1984) 699–708.
[36] F. Hayes, M. Hetherington, R. Longbottom, Mater. Sci. Technol. 6 (1990) 263–272.
[37] R. Kainuma, M. Ise, C.-C. Jia, H. Ohtani, K. Ishida, Intermetallics 4 (1996) S151–S158.
[38] G. Raynor, V. Rivlin, Equilibria in Iron Ternary Alloys, 1988, pp. 81–97.
[39] N. Kamiya, T. Sakai, R. Kainuma, I. Ohnuma, K. Ishida, Intermetallics 12 (2004) 417–423.
[40] P.B. Budberg, A. Prince, Aluminium–Iron–Nickel, in: G. Petzow, G. Effenberg (Eds.), Ternary Alloys, VCH, Weinheim, 1991, pp. 309–323.
[41] L. Zhang, Y. Du, Calphad 31 (2007) 529–540.
[42] A. Bondar, Aluminium–Cobalt–Chromium, in: G. Petzow, G. Effenberg (Eds.), Ternary Alloys, VCH, Weinheim, 1991, pp. 159–167.
[43] M. Protopopescu, H. Hubert, Aluminium–Cobalt–Nickel, in: G. Petzow, G. Effenberg (Eds.), Ternary Alloys, VCH, Weinheim, 1991, pp. 234–244.
[44] P. Rogl, Aluminium–Chromium–Nickel, in: G. Petzow, G. Effenberg (Eds.), Ternary Alloys, VCH, Weinheim, 1991, pp. 400–415.